Biogeosciences

Biogeochemical evidence of anaerobic methane oxidation on active submarine mud volcanoes on the continental slope of the Canadian Beaufort Sea

Dong-Hun Lee[1], **Jung-Hyun Kim**[2], **Yung Mi Lee**[2], **Alina Stadnitskaia**[3], **Young Keun Jin**[2], **Helge Niemann**[4,5], **Young-Gyun Kim**[6], **and Kyung-Hoon Shin**[1]

[1]Department of Marine Sciences and Convergent Technology, Hanyang University ERICA campus, 55 Hanyangdaehak-ro, Sangnok-gu, Ansan-si, Gyeonggi-do 426-791, South Korea
[2]KOPRI Korea Polar Research Institute, 26 Songdomirae-ro, Yeonsu-gu, Incheon 21990, South Korea
[3]European Council for Maritime Applied R&D, Rue Marie de Bourgogne 52–54, 1000 Brussels, Belgium
[4]NIOZ Royal Netherlands Institute for Sea Research, Department of Marine Microbiology and Biogeochemistry, NL1790 AB Den Burg, Texel, the Netherlands
[5]CAGE Centre for Arctic Gas Hydrate, Environment and Climate, Department of Geology, UiT The Arctic University of Norway, 9037 Tromsø, Norway
[6]Research Institute for Earth Resources, Kangwon National University, Chuncheon 24341, South Korea

Correspondence: Jung-Hyun Kim (jhkim123@kopri.re.kr) and Kyung-Hoon Shin (shinkh@hanyang.ac.kr)

Abstract. In this study, we report lipid biomarker patterns and phylogenetic identities of key microbial communities mediating anaerobic oxidation of methane (AOM) in active mud volcanoes (MVs) on the continental slope of the Canadian Beaufort Sea. The carbon isotopic compositions (δ^{13}C) of sn-2- and sn-3-hydroxyarchaeol showed the highly ^{13}C-depleted values (-114‰ to -82‰) associated with a steep depletion in sulfate concentrations within 0.7 m of sediment depths. This suggested the presence of methanotrophic archaea involved in sulfate-dependent AOM, albeit in a small amount. The ratio of sn-2-hydroxyarchaeol to archaeol (>1) and operational taxonomic units (OTUs) indicated that the anaerobic methanotrophic archaea (ANME) clades ANME-2c and ANME-3 were involved in AOM. Higher δ^{13}C values of archaeol and biphytanes (BPs; -55.2 ± 10.0‰ and -39.3 ± 13.0‰, respectively) suggested that archaeal communities were also assimilating AOM-derived inorganic carbon. Furthermore, the distinct distribution patterns of methanotrophs in the three MVs appears to be associated with varying intensities of ascending gas fluids. Consequently, our results suggest that the niche diversification of active mud volcanoes has shaped distinct archaeal communities that play important roles in AOM in the Beaufort Sea.

1 Introduction

Mud volcanoes (MVs) are kilometer-scale, low-temperature, seepage-related geomorphological features that provide some of the most remarkable indications of fluid venting (Ivanov et al., 1998). The roots of MVs can reach depths of up to 20 km (Shnukov et al., 2005); thus they provide key information about the geological history of the area and its possible hydrocarbon potential (Ivanov et al., 1992, 1998). Comprehensive investigations of numerous on- and offshore MV provinces have revealed the overwhelming input of hydrocarbon gases in their formation. Eruptions often manifest as a catastrophic emission of fluids consisting of hydrocarbon gases (especially methane), hydrogen sulfide, carbon dioxide, petroleum products, water, and a complex mixture of sediments, so-called "mud breccia" (Akhmanov, 1996; Akhmanov and Woodside, 1998; Ivanov et al.,1998). The occurrence of active MVs could constitute a significant portion of the geological sources of global atmospheric methane emissions (Kopf, 2002; Milkov et al., 2003). In the Arctic Ocean, where the temperature of the bottom water has been increasing (Levitus et al., 2000; Westbrook et al., 2009; Polyakov et al., 2010), concern has been raised that

the warming water will cause the disintegration of sediment-bound methane gas hydrates (Marín-Moreno et al., 2016). That would lead to higher methane concentrations and fluxes in surface sediments; thus the ascending methane would quickly be released into the water column and potentially the atmosphere (Niemann et al., 2006; Felden et al., 2010). The submarine MVs are therefore of considerable interest in global warming scenarios, since methane is a greenhouse gas that is > 20 times more potent than carbon dioxide (Wuebbles and Hayhoe, 2002; Etminan et al., 2016). Accordingly, MV sediments can be regarded as a model system for studying the biogeochemical dynamics of sediments characterized by high methane fluxes.

Across the Canadian Beaufort continental slope, active MVs were discovered at water depths of ∼ 282, ∼ 420, and ∼ 740 m during the multibeam bathymetric mapping surveys conducted in 2009 and 2010 (Campbell et al., 2009). They were named with respect to their water depths, i.e., MV282, MV420, and MV740 (Blasco et al., 2013; Saint-Ange et al., 2014). Previous investigations based on sediment coring and mapping with an autonomous underwater vehicle (AUV) and a remotely operated vehicle (ROV) showed that these MVs are young and active edifices characterized by ongoing eruptions (Paull et al., 2015). The gas ascending via these MVs consists of > 95 % methane with $\delta^{13}C_{CH_4}$ values of −64‰ (Paull et al., 2015), indicating a microbial methane source (Whiticar, 1999). Siboglinid tube worms and white bacteria mats were reported at MV420 (Paull et al., 2015). Those organisms typically consume sulfide and are thus often associated with elevated anaerobic methanotrophy in near-surface sediments, because sulfide is an end product of the anaerobic oxidation of methane (AOM) with sulfate as the terminal electron acceptor (Boetius and Wenzhöfer, 2013; Paull et al., 2015). AOM is mediated by several clades of anaerobic methanotrophic archaea (ANME) that typically form syntrophic associations with sulfate-reducing partner bacteria (Knittel and Boetius, 2009). This process is represented by the following:

$$CH_4 + SO_4^{2-} \rightarrow HCO_3^- + HS^- + H_2O. \qquad (1)$$

A powerful tool to investigate AOM communities in sediments is the analysis of membrane lipids combined with their compound-specific carbon isotopic composition (^{13}C), which can be used to chemotaxonomically infer community composition (Niemann and Elvert, 2008, and references therein). In particular, low ^{13}C values in AOM-derived lipids are widely used to trace AOM in ancient (e.g., Zhang et al., 2003; Stadnitskaia et al., 2008a, b; Himmler et al., 2015) and modern seep settings (e.g., Hinrichs and Boetius, 2002; Niemann et al., 2005; Chevalier et al., 2011, 2014). Although the ebullition of methane from the Beaufort Sea MVs has been documented before (Paull et al., 2015), the sediment methane dynamics, including the role of AOM as a barrier against rising methane in these systems, have not been investigated.

In this study, we thus investigated three sediment cores recovered from active MVs on the continental slope of the Canadian Beaufort Sea during the ARA05C expedition with the R/V *ARAON* in 2014. By using a combination suite of lipid and nucleic acid analyses with bulk geochemical parameters, our study sheds light on the specific archaeal communities involved in AOM at active MVs in the Canadian Beaufort Sea.

2 Material and methods

2.1 Sample collection

Three sediment cores were recovered using a gravity corer during the ARA05C expedition of the South Korean icebreaker R/V *ARAON* in the Canadian Beaufort Sea in August 2014 (Fig. 1a–c). Core ARA05C-10-GC (70°38.992′ N, 135°56.811′ W; 282 m water depth, 221 cm core length), core ARA05C-01-GC (70°47.342′ N, 135°33.952′ W; 420 m water depth, 272 cm core length), and core ARA05C-18-GC (70°48.082′ N, 136°05.932′ W; 740 m water depth, 300 cm core length) were retrieved from the active MV sites MV282, MV420, and MV740, respectively. Upon recovery, all sediment cores showed active degassing (Fig. 1d). When the sediment cores were split, we observed a mousse-like texture in cores ARA05C-10-GC and ARA05C-01-GC, related to outgassing as a result of the pressure change during recovery. Gas hydrates in the shape of isolated veins with a thickness of about ≤ 2 cm were observed at the bottom (230 to 300 cm) of core ARA05C-18-GC. The split sediment cores were lithologically described and then subsampled for total organic carbon (TOC), lipid biomarkers, and 16S ribosomal ribonucleic acid (16S rRNA) gene sequences on board. After subsampling, sediment samples were stored at −20 °C for geochemical analyses and at −80 °C for microbial analyses.

2.2 Bulk geochemical analysis

Sediment samples were freeze-dried and homogenized using an agate mortar prior to the TOC analyses. Sediment samples (∼ 1 g) were then treated with 8 mL 1N HCl to remove carbonates before measuring the TOC content and its isotopic composition using an elemental analyzer (EuroEA3028, Eurovector, Milan, Italy) connected to an isotope ratio mass spectrometer (IsoPrime, GV Instruments, Manchester, UK). All isotope ratios of TOC are reported using the δ-notation (per mill) with respect to the Vienna Pee Dee Belemnite (VPDB). The analytical errors (standard deviations of repeated measurements of the internal standard CH6 certified by the International Atomic Energy Agency – IAEA) were smaller than ±0.1 wt % for TOC and ±0.1‰ for $\delta^{13}C_{TOC}$.
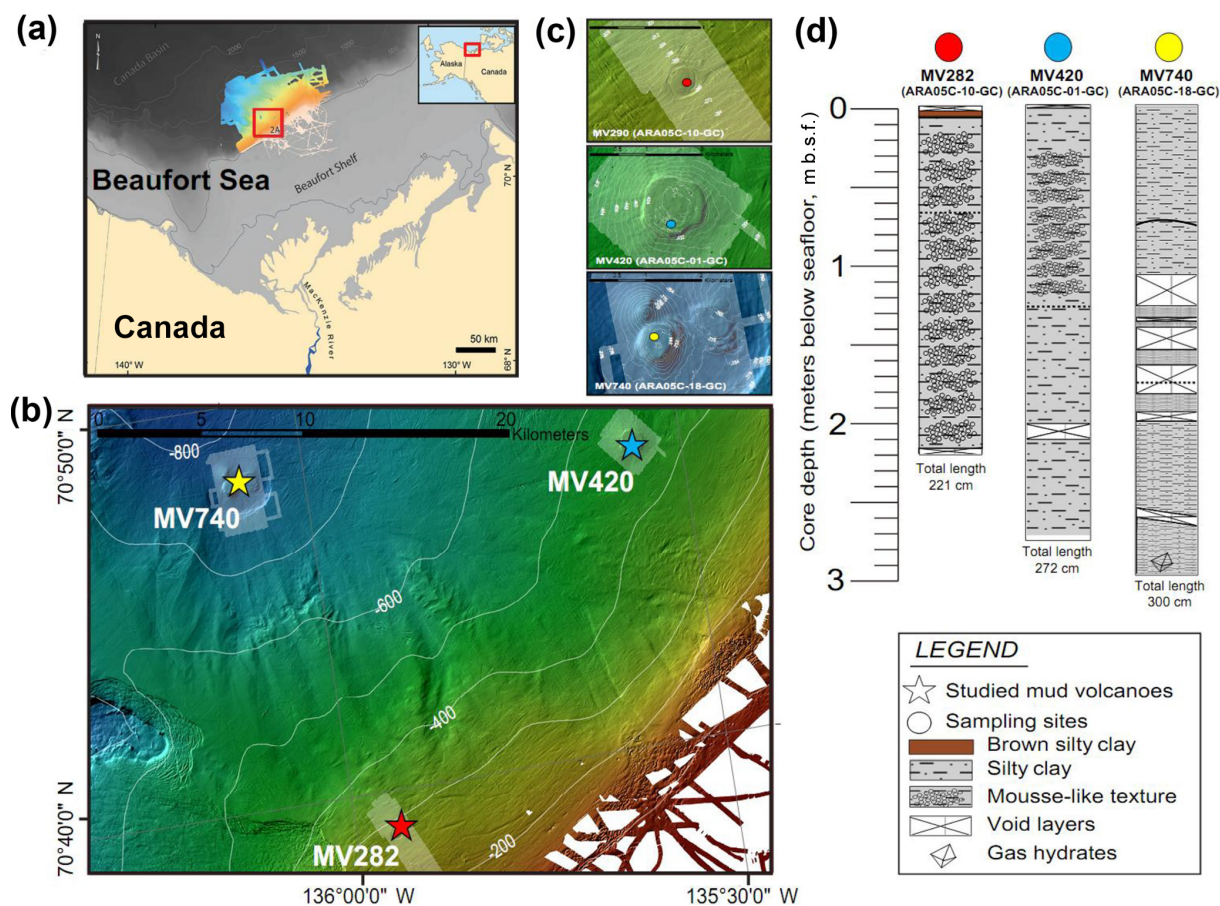
Figure 1. (a) Map showing the study area (red box) with inset regional map of Alaska and northwestern Canada modified from Paull et al. (2015). **(b)** Map showing the three mud volcano (MV) locations on the upper slope of the Beaufort Sea. **(c)** Detailed bathymetric maps showing the locations of sediment cores ARA05C-10-GC (MV282), ARA05C-01-GC (MV420), and ARA05C-18-GC (MV740). **(d)** Lithology of the three sediment cores investigated.

2.3 Lipid extraction and purification

The homogenized sediment samples (ca. 10 g) were extracted with an accelerated solvent extractor (Dionex ASE 200, Dionex Corporation, Sunnyvale, CA, USA) using a solvent mixture of $9 : 1$ ($v : v$) dichloromethane (DCM) to methanol (MeOH) at a temperature of $100\,°C$ and a pressure of 7.6×10^6 Pa. The total lipid extract was dried over anhydrous Na_2SO_4 and was treated with tetrabutylammonium sulfite reagent to remove elemental sulfur. An aliquot was chromatographically separated into apolar and polar fractions over an Al_2O_3 (activated for 2 h at $150\,°C$) column with solvents of increasing polarity. The apolar fraction was eluted using hexane : DCM ($9 : 1$, $v : v$), and the polar fraction was recovered with DCM : MeOH ($1 : 1$, $v : v$) as an eluent. After column separation, $40\,\mu L$ of 5α-androstane ($10\,\mu g\,mL^{-1}$) was added to the apolar fraction as an internal standard. The polar fraction was divided into two aliquots, to which either C_{22} 7,16-diol ($10\,\mu g\,mL^{-1}$) or C_{46} glycerol dialkyl glycerol tetraethers (GDGTs; $10\,\mu g\,mL^{-1}$)

were added as an internal standard. Half of the polar fraction containing C_{22} 7,16-diol was dried and silylated with $25\,\mu L$ N,O-bis(trimethylsilyl)trifluoroacetamide (BSTFA) and $25\,\mu L$ pyridine before heating it to $60\,°C$ for 20 min to form trimethylsilyl derivatives. The second half of the polar fraction containing C_{46} GDGT was redissolved by sonication (5 min) in hexane : isopropanol ($99 : 1$, $v : v$) and then filtered with a $0.45\,\mu m$ polytetrafluoroethylene filter. Afterwards, an aliquot of the filtered fraction was treated with HI following the procedure described by Kaneko et al. (2011) in order to cleave ether bonds from GDGTs, thereby releasing biphytanes (BPs) which can be analyzed by a gas chromatographer (GC).

2.4 Identification and quantification of lipid biomarkers

All apolar and polar fractions were analyzed using a Shimazu GC (Shimazu Corporation, Kyoto, Japan) equipped with a splitless injector and a flame ionization detector for com-

pound quantification. A fused silica capillary column (CP-sil 5 CB, 25 m length, 0.32 mm internal diameter – i.d., and 0.12 μm film thickness) was used with He (1.3 mL min^{-1}) as a carrier gas. The samples were injected under constant flow at an initial oven temperature of 70 °C. The GC oven temperature was subsequently raised to 130 °C at a rate of 20 °C min^{-1}, and then to 320 °C at 4 °C min^{-1}, with a final hold time of 15 min. Concentrations were obtained by comparing the peak area of each compound with that of 5α-androstane for the apolar fraction and C$_{22}$ 7,16-diol for the polar fraction. Compound identifications for the apolar, silylated, and BP polar fractions were conducted using a Shimazu GC connected to a GCMS-QP2010 mass spectrometer (MS) operated at 70 eV (cycle time of 0.9 s, resolution of 1000) with a mass range of m/z 50–800. The samples were subjected to the same temperature conditions and capillary column described for GC analysis. Molecular structures were determined by comparing their mass spectral fragmentation patterns and retention times with previously published data.

An aliquot of the filtered polar fractions was analyzed by high-performance liquid chromatography–atmospheric-pressure positive-ion chemical ionization–mass spectrometry (HPLC-APCI-MS) using an Agilent 6120 Series LC/MSD SL system (Agilent Technologies, Santa Clara, CA, USA) equipped with an auto-injector and Chemstation chromatography manager software. Separation was achieved on two UHPLC silica columns (BEH HILIC columns, 150 mm length, 2.1 mm i.d., 1.7 μm particle size), fitted with precolumns (5 mm length, 2.1 mm i.d.) of the same material and maintained at 30 °C. Injection volumes varied from 1 L. GDGTs were eluted isocratically, with 82 % A and 18 % B for 25 min, followed by a linear gradient to 35 % B over 25 min, then to 100 % B over 30 min, and finally maintained for 20 min, where A represents hexane and B represents hexane : 2-propanol (90 : 10, $v : v$). The flow rate was 0.2 mL min^{-1}, with a total run time of 90 min. After each analysis, the column was cleaned by back-flushing hexane : 2-propanol (90 : 10, $v : v$) at 0.2 mL min^{-1} for 20 min. Conditions for APCI-MS were as follows: nebulizer pressure of 60 psi, vaporizer temperature of 400 °C, a drying gas (N$_2$) flow of 6 mL min^{-1} and temperature of 200 °C, capillary voltage of −3.5 kV, and a corona of 5 μA ($\sim$ 3.2 kV). Detection was achieved in the single ion monitoring of [M + H]$^+$ ions (dwell time 35 ms), as described by Schouten et al. (2007). GDGTs were quantified by integrating peak areas and using the internal standard according to Huguet et al. (2006).

2.5 Compound-specific stable carbon isotope analysis

The δ^{13}C values of selected compounds were determined by GC–combustion–isotope ratio mass spectrometry (GC–C–IRMS), as described by Kim et al. (2017). An IRMS (IsoPrime, GV Instruments, UK) was connected with a GC (Hewlett Packard 6890 N series, Agilent Technologies, Santa

Clara, CA, USA) via a combustion interface (glass tube packed with copper oxide – CuO, operated at 850 °C). The samples were subjected to the same temperature conditions and capillary column described for the GC and GC-MS analyses. Calibration was performed by injecting several pulses of reference gas CO$_2$ of the known δ^{13}C value at the beginning and the end of each sample run. Isotopic values are expressed as δ^{13}C values in per mill relative to the VPDB. The δ^{13}C values were further corrected using a certified isotope standard (Schimmelmann alkane mixture type A6, Indiana University). The correlation coefficients (r^2) of the known δ^{13}C values of certified isotope standards with the average values of the measured samples were higher than 0.99. In the case of the silylation of alcohols, we corrected the measured δ^{13}C values for the isotopic composition of the methyl adducts (the δ^{13}C value of the BSTFA is -19.3 ± 0.5‰). In order to monitor the accuracy of the measurements, standards with known δ^{13}C values were repeatedly analyzed for every 5–6 sample run. Standard deviations of carbon isotope measurements were generally better than ± 0.4‰, as determined by repeated injections of the standard.

2.6 Genomic DNA extraction and amplification of 16S rRNA genes

Sediment samples stored at -80 °C were freeze-dried, and genomic DNA was extracted from ~ 0.5 g of freeze-dried samples using the FastDNA Spin Kit for Soil (QBiogene, Carlsbad, CA, USA). The 16S rRNA gene was amplified by a polymerase chain reaction (PCR) using the 8F (3-CTCAGAGTAGTCCGGTTGATCCYGCCGG-5′) / 519R (3′-ACAGAGACGAGGTDTTACCGCGGCKGCTG-5′) primers with barcodes for archaeal community analysis. PCR was carried out with 30 μL of reaction mixture containing DreamTaq Green PCR Master Mix (2×; Thermo Fisher Scientific, Waltham, MA, USA), 1 μL of 5 μM primers, and 4 μL of genomic DNA. The PCR procedure included an initial denaturation step at 94 °C for 3 min, 30 cycles of amplification (94 °C for 1 min, 55 °C for 1 min, and 72 °C for 1.5 min), and a final extension step at 72 °C for 5 min. Each sample was amplified in triplicate and pooled. PCR products were purified using the LaboPass purification kit (Cosmo Genetech, Seoul, South Korea). Due to PCR failure for samples below 0.6 m in the MV740 sample, these samples were not included in further analysis.

2.7 Archaeal community and phylogenetic analysis

Sequencing of the 16S rRNA amplicon was carried out by Chun Lab (Seoul, South Korea) using a 454 GS FLX Titanium sequencing machine (Roche, Branford, CT, USA). Pre-processing and de-noising were conducted using a PyroTrimmer (Oh et al., 2012). Sequences were processed to remove primer, linker, and barcode sequences. The 3′ ends of sequences with low-quality values were trimmed when the av-

erage quality score for a 5 base-pair window size was lower than 20. Sequences with ambiguous nucleotides and those shorter than 250 bp were discarded. Chimeric reads were detected and discarded using the de novo chimera detection algorithm UCHIME (Edgar et al., 2011). Sequence clustering was performed using CLUSTOM (Hwang et al., 2013) with a 97 % similarity cutoff. Taxonomic assignment was conducted for representative sequences of each cluster by an EzTaxon-e database search (Kim et al., 2012). Raw reads were submitted to the National Center for Biotechnology Information (NCBI) Sequence Read Archive (SRA) database (accession number PRJNA433786).

For phylogenetic analysis of operational taxonomic units (OTUs) based on 16S rRNA genes, we selected OTUs belonging to the class Methanomicrobia that composed more than 1 % of the relative abundance and aligned them with those of Methanomicrobia in jPHYDIT. A phylogenetic tree was constructed using the maximum likelihood algorithm (Felsenstein et al., 1981) with MEGA 6 (Tamura et al., 2013). The robustness of the tree topologies was assessed by bootstrap analyses based on 1000 replications of the sequences.

3 Results

3.1 Bulk geochemical and microbial lipid analyses

Dissolved sulfate concentrations in sediment cores from MV282, MV420, and MV740 ranged from 0.1 to 26.8 mM and sharply decreased within 0.7 m in core depths (Fig. 2; see also Paull et al., 2015). Overall, the TOC contents of core sediments from MV282, MV420, and MV740 ranged from 1.2–1.5 wt %, 1.0–1.3 wt %, and 1.1 wt %–1.3 wt %, respectively (Fig. 2; see also Table 1). Similarly, $\delta^{13}C_{TOC}$ values in MV282, MV420, and MV740 cores showed little variation, with average values of -26.3 ± 0.07‰, -26.2 ± 0.05‰, and -26.3 ± 0.06‰, respectively (Fig. 2; see also Table 1).

Isoprenoid dialkyl glycerol diethers (DGDs), considered as biomarkers diagnostic for ANMEs such as archaeol (2,3-di-O-phytanyl-sn-glycerol) and sn-2-hydroxyarchaeol (2-O-3-hydroxyphytanoyl-3-O-phytanyl-sn-glycerol), were identified in the polar fractions of all three cores (Fig. S1 in the Supplement); their concentrations were 0.03–0.09 µg g^{-1} and 0.01–0.13 µg g^{-1}, respectively (Fig. 3; see also Table 1). sn-3-hydroxyarchaeol was identified only in MV282 and MV420 sediments at concentrations of 0.01–0.08 µg g^{-1} (Fig. 3; see also Table 1). Among non-isoprenoid DGDs, we identified DGD (If) with $anteiso$ pentadecyl moieties attached at both the sn-1 and sn-2 positions in all three cores. The concentrations of non-isoprenoid DGD (If) ranged from 0.06 to 0.25 µg g^{-1} (Fig. 3; see also Table 1). Isoprenoid GDGTs containing zero to three cyclopentane moieties (GDGT-0 to GDGT-3) and crenarchaeol which, in addition to four cyclopentane moieties, contains a cyclohexane moiety, were detected in all samples investigated (Fig. 4).

Figure 2. Depth profiles of sulfate (SO_4^{2-}) concentrations, total organic carbon (TOC) content, and $\delta^{13}C_{TOC}$ in sediment cores from MV282, MV420, and MV740. Grey hatched bars indicate gas gaps in the sediment layers. Note that the sulfate concentration data are from Paull et al. (2015).

Overall, the isoprenoidal GDGTs were dominated by GDGT-0 and crenarchaeol, with concentrations of 0.02–0.19 µg g^{-1} and 0.02–0.25 µg g^{-1}, respectively, whereas GDGT-1 and GDGT-2 showed much lower concentrations (≤ 0.02 µg g^{-1}) in the three cores. In the apolar fractions, we did not detect any isoprenoid hydrocarbons that are typically associated with ANMEs, i.e., the C$_{20}$ compound 2,6,11,15-tetramethylhexadecane (crocetane) or the C$_{25}$ compound 2,6,10,15,19-pentamethylicosane (PMI).

At the three MVs, the $\delta^{13}C$ values of archaeol and sn-2-hydroxyarchaeols ranged from -79.8‰ to -38.5‰ and from -113.9‰ to -82.1‰, respectively (Fig. 3; Table 1). The $\delta^{13}C$ values of sn-3-hydroxyarchaeol were as low as -93.1‰. The $\delta^{13}C$ values of the non-isoprenoid DGD (If) varied between -46.9‰ and -31.9‰. The $\delta^{13}C$ values

Table 1. Results of total organic carbon (TOC) contents, $\delta^{13}C$ of TOC, and concentrations and stable carbon isotopes of selected lipid biomarkers such as isoprenoid DGDs, non-isoprenoid DGDs, and biphytanes derived from isoprenoid GDGTs.

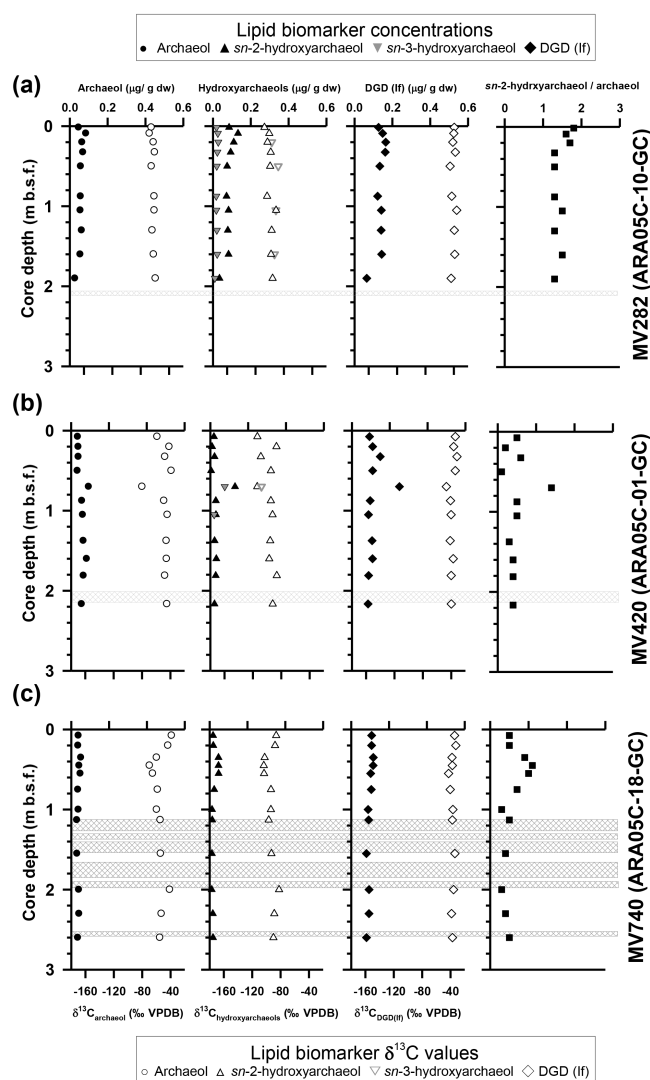| Core depth (m b.s.f.)	TOC (wt %)	$\delta^{13}C_{TOC}$ (‰ VPDB)	Archaeol μg g⁻¹ dw	Archaeol ‰ VPDB	sn-2-hydroxyarchaeol μg g⁻¹ dw	sn-2-hydroxyarchaeol ‰ VPDB	sn-3-hydroxyarchaeol μg g⁻¹ dw	sn-3-hydroxyarchaeol ‰ VPDB	Non-isoprenoid DGDs μg g⁻¹ dw	Non-isoprenoid DGDs ‰ VPDB	GDGT-0 μg g⁻¹ dw	GDGT-1 μg g⁻¹ dw	GDGT-2 μg g⁻¹ dw	GDGT-3 μg g⁻¹ dw	Crenarchaeol μg g⁻¹ dw	Biphytane 0 ‰ VPDB	Biphytane 1 ‰ VPDB	Biphytane 2 ‰ VPDB	Biphytane 3 ‰ VPDB	hydroxyarchaeol and archaeol
MV282																				
0.02	1.2	−26.6	0.05	−65.0	0.09	−107.4	0.02	n.d.	0.13	−39.4	0.07	0.01	0.01	0.00	0.09	−29.4	−46.2	−39.0	−27.1	1.8
0.09	1.5	−26.6	0.09	−67.7	0.13	−100.6	0.03	n.d.	0.15	−40.1	0.08	0.01	0.01	0.01	0.08	−32.3	−63.4	−30.9	−26.8	1.6
0.20	1.1	−26.4	0.06	−62.0	0.11	−103.2	0.03	−92.8	0.16	−41.4	0.06	0.01	0.01	0.01	0.06	−33.9	−46.3	−28.6	−26.6	1.7
0.33	1.2	−26.2	0.07	−60.3	0.09	−98.6	0.02	−84.2	0.16	−37.9	0.05	0.01	0.00	0.00	0.05	—	—	—	—	1.3
0.50	1.3	−26.2	0.06	−64.8	0.07	−99.4	0.02	−93.1	0.13	−45.3	0.05	0.01	0.01	0.01	0.05	−36.4	n.d.	−21.2	−29.6	1.3
0.88	1.5	−26.0	0.06	−60.9	0.07	−103.6	0.02	n.d.	0.12	−42.9	0.05	0.01	0.00	0.00	0.05	—	−36.0	−29.0	−16.7	1.3
1.05	1.4	−26.2	0.06	−60.8	0.08	−91.0	0.02	−87.3	0.14	−36.0	0.05	0.01	0.00	0.00	0.06	−32.2	—	—	—	1.5
1.30	1.4	−26.2	0.06	−63.7	0.08	−97.3	0.02	n.d.	0.14	−39.3	0.05	0.01	0.01	0.00	0.05	—	—	—	—	1.5
1.60	1.5	−26.2	0.06	−61.8	0.08	−98.1	0.02	−89.1	0.14	−38.8	0.00	0.00	0.00	0.00	0.06	−33.5	−38.6	—	−37.6	1.5
1.90	1.2	−26.5	0.03	−59.2	0.03	−96.0	0.01	n.d.	0.06	−43.8	0.02	0.00	0.00	0.00	0.02	—	—	—	—	1.3
MV420																				
0.08	1.0	−26.4	0.03	−58.6	0.02	−113.8	n.d.	n.d.	0.09	−34.3	0.12	0.01	0.01	0.01	0.07	−42.7	n.d.	n.d.	n.d.	0.5
0.20	1.1	−26.3	0.04	−41.7	0.01	−86.8	n.d.	n.d.	0.11	−36.6	0.19	0.02	0.01	0.01	0.12	−34.0	−61.6	−22.9	−24.0	0.2
0.33	1.1	−26.2	0.04	−47.6	0.02	−108.8	n.d.	n.d.	0.15	−31.9	0.06	0.00	0.00	0.00	0.05	−61.6	—	—	—	0.6
0.50	1.1	−26.1	0.03	−38.6	0.00	−94.6	n.d.	n.d.	0.11	−34.3	0.03	0.00	0.00	0.00	0.02	−30.3	−51.4	−28.4	−24.0	0.1
0.70	1.1	−26.7	0.09	−79.8	0.13	−113.9	0.08	−93.1	0.25	−46.9	0.10	0.01	0.01	0.01	0.13	−51.4	—	—	—	1.4
0.88	1.2	−26.2	0.06	−49.0	0.03	−94.7	0.02	n.d.	0.10	−41.0	0.06	0.01	0.01	0.01	0.04	—	−55.7	−30.1	−30.4	0.5
1.05	1.2	−26.0	0.06	−44.2	0.03	−92.4	n.d.	n.d.	0.09	−40.2	0.07	0.01	0.01	0.01	0.06	−32.3	−55.7	−30.1	−30.4	0.5
1.38	1.1	−26.1	0.06	−45.6	0.02	−95.7	n.d.	n.d.	0.11	−41.5	0.07	0.01	0.01	0.01	0.06	−55.7	—	—	—	0.3
1.6	1.2	−26.1	0.08	−45.3	0.03	−97.0	n.d.	n.d.	0.11	−37.2	0.08	0.01	0.01	0.01	0.07	−46.8	−46.8	−29.4	−28.2	0.4
1.81	1.2	−26.0	0.07	−47.7	0.03	−86.4	0.02	−89.1	0.09	−40.1	0.30	0.04	0.05	0.03	0.25	−34.8	−50.5	−27.0	−23.5	0.4
2.17	1.3	−26.1	0.06	−44.8	0.02	−92.1	0.01	n.d.	0.09	−39.9	0.27	0.03	0.04	0.03	0.22	—	—	—	—	1.3
MV740																				
0.08	1.2	−26.3	0.04	−38.5	0.02	−86.2	n.d.	n.d.	0.11	−34.3	0.07	0.01	0.01	0.01	0.05	−36.2	−49.5	−26.8	−25.3	0.5
0.20	1.1	−26.3	0.04	−43.6	0.02	−87.8	n.d.	n.d.	0.11	−32.6	0.07	0.01	0.01	0.01	0.05	—	—	—	—	0.5
0.35	1.3	−26.4	0.05	−59.6	0.05	−102.4	n.d.	n.d.	0.12	−37.9	0.09	0.01	0.01	0.01	0.07	−36.1	−57.0	−24.6	−31.7	0.9
0.45	1.1	−26.4	0.04	−69.6	0.05	−103.7	n.d.	n.d.	0.12	−37.5	0.09	0.01	0.01	0.01	0.06	−31.5	−56.0	−25.2	−31.4	1.1
0.55	1.2	−26.5	0.05	−65.1	0.05	−103.3	n.d.	n.d.	0.10	−42.7	0.06	0.01	0.01	0.01	0.05	−40.5	−50.6	−27.2	−30.7	1.0
0.75	1.1	−26.2	0.04	−58.3	0.02	−93.5	n.d.	n.d.	0.11	−40.4	0.08	0.01	0.01	0.01	0.05	−31.0	−55.5	−31.4	−26.8	0.7
1.00	1.2	−26.1	0.04	−59.5	0.01	−93.7	n.d.	n.d.	0.09	−36.7	0.09	0.01	0.01	0.01	0.07	—	—	—	—	0.3
1.13	1.1	−26.2	0.03	−54.4	0.01	−96.7	n.d.	n.d.	0.09	−37.4	0.08	0.01	0.01	0.01	0.05	—	—	—	—	0.5
1.55	1.3	−26.2	0.03	−53.9	0.01	−93.0	n.d.	n.d.	0.09	−33.8	0.07	0.01	0.01	0.01	0.05	—	—	—	—	0.5
2.00	1.2	−26.2	0.03	−41.2	0.01	−82.1	n.d.	n.d.	0.09	−35.7	0.08	0.01	0.01	0.01	0.06	−33.4	−50.5	−27.0	−23.5	0.4
2.30	1.2	−26.3	0.04	−52.8	0.02	−88.8	n.d.	n.d.	0.09	−38.6	0.08	0.01	0.01	0.01	0.06	—	—	—	—	0.4
2.60	1.1	−26.4	0.03	−55.0	0.02	−90.1	n.d.	n.d.	0.08	−37.3	0.06	0.01	0.01	0.01	0.05	−34.1	n.d.	n.d.	n.d.	0.5

n.d. – not detected.

Figure 3. Vertical profiles of selected lipid biomarkers (archaeol, hydroxyarchaeol, and DGD – If) obtained from sediment cores **(a)** ARA05C-10-GC (MV282), **(b)** ARA05C-01-GC (MV420), and **(c)** ARA05C-18-GC (MV740). Grey hatched bars indicate gas gaps in sediment layers.

of BPs derived from the isoprenoid GDGTs ranged from -63.4‰ to -16.7‰. The $\delta^{13}C$ values of BP-1 (on average -51.0‰) were slightly more depleted than those of BP-0 (on average -34.2‰), BP-2 (on average -28.3‰), and BP-3 (on average -27.5‰).

3.2 Depth profile of archaeal communities

Archaeal communities were phylogenetically classified as the taxonomic level of class (Table S1 and Fig. S2). The archaeal classes detected were Miscellaneous Crenarchaeota Group (MCG)_c, Methanomicrobia, South African Gold Mine Euryarchaeotic Group Mediterranean Sea Brine Lakes (SAGMEGMSBL_c), Thermoplasmata, Lokiar-

chaeota_c (formerly Marine Benthic Group B), Marine Hydrothermal Vent Group 3 (MHVG3_c), Group 1a_c, and Group 1b_c. MCG_c of the phylum Bathyarchaeota was the most dominant archaeal class at the three MVs at a range of depths, with the exception of the surface of MV420, accounting for 39.7 % to 99.2 % of the total archaeal sequences. In contrast to the archaeal communities below 0.3 m in MV282 and 1.1 m in MV420, which were dominated by MCG_c, shallow archaeal communities at depths of 0.0–0.2 m at MV282, 0.1–0.7 m at MV420, and 0.1–0.6 m at MV740, had different compositions in the MVs. The class Methanomicrobia represented a relatively high proportion (up to 20.9 %) in these shallow depths at all three MVs.

4 Discussion

4.1 Signals of AOM activity in Beaufort Sea mud volcanoes

Active gas bubble emissions into the overlying water column have previously been observed at all the investigated MVs, i.e., MV282, MV420, and MV740 (Paull et al., 2011, 2015). A sharp decrease in pore water sulfate concentration and a rapid increase in sediment temperature near the seafloor indicates the ascension of sulfate-depleted, warm fluids containing methane from these MVs (Paull et al., 2015). Thus, several lines of evidence suggest that interstitial methane gas is likely saturated near the seafloor of the investigated MVs, meaning that both an electron acceptor (sulfate) and a donor (methane) for AOM are present in the near-surface sediments. Furthermore, an indirect indication of AOM in near-surface sediments is the presence of thiotrophic organisms, i.e., siboglinid tube worms closely related to *Oligobrachia haakonmosbiensis* and the white bacterial mats found at the summit of MV420 (Paull et al., 2015). Such thiotrophs, which consume the AOM end product, sulfide, are typically found in habitats characterized by high AOM activity in the near-surface sediments (Niemann et al., 2006; Rossel et al., 2011; Felden et al., 2014).

AOM at active methane seeps typically proceeds with sulfate as the terminal electron acceptor (Boetius et al., 2000; Reeburgh, 2007; Knittel et al., 2009; James et al., 2016), although recent research also found indications for AOM with electron acceptors other than sulfate, i.e., oxidized Mn and Fe species (Beal et al., 2009) or nitrate and/or nitrite (Haroon et al., 2013). The key microbial communities involved in sulfate-dependent AOM are ANMEs in association with sulfate reducing partner bacteria (Knittel et al., 2009), although ANMEs may also mediate sulfate-dependent AOM without bacterial partners (Milucka et al., 2012). AOM with alternative electron acceptors in marine settings is probably mediated by specialized ANMEs (Beal et al., 2009; Haroon et al., 2013), but it remains unclear how far potential bacterial partners are involved in these processes. At the MVs

investigated here, we found indications for sulfate–methane transition zones (SMTZ), because sulfate penetrated only about 0.20 (MV270), 0.20 (MV420), and 0.45 m (MV740) into the seafloor, and we found corresponding elevated abundances of sulfate-dependent AOM communities and their lipid biomarkers (Fig. 2; see also discussion on AOM communities in sediments in Sect. 4.2). In contrast to sulfate, the other potential electron acceptors for the AOM mentioned above are typically depleted at shallow depths because redox reactions are more thermodynamically feasible than AOM (Reeburgh, 2007). We did not detect any of the archaeal communities (i.e., *Methanoperedens nitroreducens*; Haroon et al., 2013) that mediate AOM with electron acceptors other than sulfate, which makes alternative modes of AOM at the investigated MVs rather unlikely.

4.2 Contribution of AOM to sedimentary biomass

AOM-derived biomass (including lipids) is generally depleted in ^{13}C compared to the ^{13}C values of source methane as a result of isotopic fractionation during methane assimilation (Whiticar, 1999). As AOM-related biomarkers, we found substantial amounts of *sn*-2-hydroxyarchaeol among the isoprenoid DGDs in all three MV sediment cores (Fig. 3). *sn*-3-hydroxyarchaeol, an isomer of *sn*-2-hydroxyarchaeol (e.g., Pancost et al., 2000; Elvert et al., 2005; Niemann et al., 2005; Bradley et al., 2009), was also detected in MV282 but not in MV420 or MV740, except at 0.7 m in MV420 (Fig. 3). The δ^{13}C values of *sn*-2-hydroxyarchaeol were more depleted than the $\delta^{13}C_{CH_4}$ values (by about −64 ‰; Paull et al., 2015), with average $\Delta\delta^{13}$C values (lipid methane) of −35.5 ‰ in MV282, −33.8 ‰ in MV420, and −29.5 ‰ in MV740. Notably, the $\Delta\delta^{13}$C values of *sn*-2-hydroxyarchaeol were slightly larger in MV282 than in the other MVs. Similar to *sn*-2-hydroxyarchaeol, the δ^{13}C values of *sn*-3-hydroxyarchaeol in the MV sediments were generally more depleted than the $\delta^{13}C_{CH_4}$ values. Accordingly, the depleted δ^{13}C values of *sn*-2- and *sn*-3-hydroxyarchaeol indicated recent AOM occurrence in sediment where sulfate was present. On the other hand, the depleted δ^{13}C values of *sn*-2-hydroxyarchaeol detected below the SMTZ were likely a fossil AOM signature (Lee et al., 2013). Non-isoprenoid DGD (If), identified as a robust marker of sulfate-reducing bacteria (SRB) involved in AOM (e.g., Pancost et al., 2001a; Werne et al., 2002), was detected throughout all three MV sediment cores (Fig. 3). However, the δ^{13}C values of the non-isoprenoid DGD (If; −46.9 ‰ to −32.6 ‰) were enriched in ^{13}C relative to the ascending methane in the MVs. Therefore, our δ^{13}C data from the non-isoprenoid DGD (If) suggest that those compounds originate from a mixed community mediating AOM and other processes.

Furthermore, our measurements of the TOC content and $\delta^{13}C_{TOC}$ values in the three sediment cores revealed narrow ranges of 1.2 ± 0.1 wt % and $−26.4 \pm 0.6$ ‰, respectively (Fig. 2; see also Table 1), without the negative isotopic

excursion that has often been observed in MVs in association with methane-derived biomass from AOM (e.g., Haese et al., 2003; Werne et al., 2004). Therefore, in accordance with methane ebullition to water column (Paull et al., 2015), our bulk geochemical data suggest that the contribution of AOM biomass to sedimentary TOC was rather low at the MVs we investigated, which is in line with our findings that the non-isoprenoid GDGTs substantially originate from bacterial sources unassociated with methanotrophy.

Similarly, we found substantial amounts of archaeal lipids that originated from sources other than AOM. All sediment cores from the three MVs showed a predominance of GDGT-0 and crenarchaeol (Fig. 4), revealing the contribution of marine pelagic Thaumarchaeota (Schouten et al., 2013). The isoprenoid GDGT distributions also did not show a clear dominance of GDGT-2 over GDGT-0. The values of the GDGT-0 to crenarchaeol (Liu et al., 2011), the GDGT-2 to crenarchaeol (Weijers et al., 2011), and the methane index values (Zhang et al., 2011) were also low, with ranges of 0.8–1.7, 0.1–0.2, and 0.2–0.4, respectively. Thus, the GDGT signals found here indicate the negligible contribution of Euryarchaeota to AOM and the GDGT pool (e.g., Pancost et al., 2001b; Zhang et al., 2003; Niemann et al., 2005; Stadnitskaia et al., 2008a, b). The ^{13}C-enriched isotopic signatures of BPs (Table 1) relative to methane provide further evidence that the isoprenoid GDGTs derived from methanotrophic archaea were low in the investigated sediments. For example, at sites characterized by high AOM activity, previous studies found GDGT-1 and GDGT-2 total concentrations of up to 3 ug g^{-1}, 10-fold higher than in our results (Stadnitskaia et al., 2005). We can only speculate about the reasons for the low abundances of AOM-related archaeal communities contributing to the GDGT pool. One possibility is a rather recent onset in seepage activity at the coring sites, which would leave too little time for the slow-growing AOM communities that are characterized by doubling times on the month scale to have grown large (Nauhaus et al., 2007).

4.3 AOM-related microbial communities in Beaufort Sea mud volcanoes

4.3.1 Chemotaxonomy

The composition of microbial lipids and their δ^{13}C values can be used to infer the chemotaxonomic composition of microbes involved in sulfate-dependent AOM (Niemann and Elvert, 2008). Previously, three groups of anaerobic methanotrophic archaea (ANME-1, ANME-2, and ANME-3) have been reported in a variety of cold seep environments, which are related to methanogens on the order of Methanosarcinales and Methanomicrobiales (Knittel and Boetius, 2009). Archaeol is ubiquitous in archaea, often serving as an indicator of methanogenic archaea in a wide range of environments including MVs (e.g., De Rosa and Gambacorta, 1988; Koga et al., 1993, 1998; Pancost et al., 2011). In contrast,
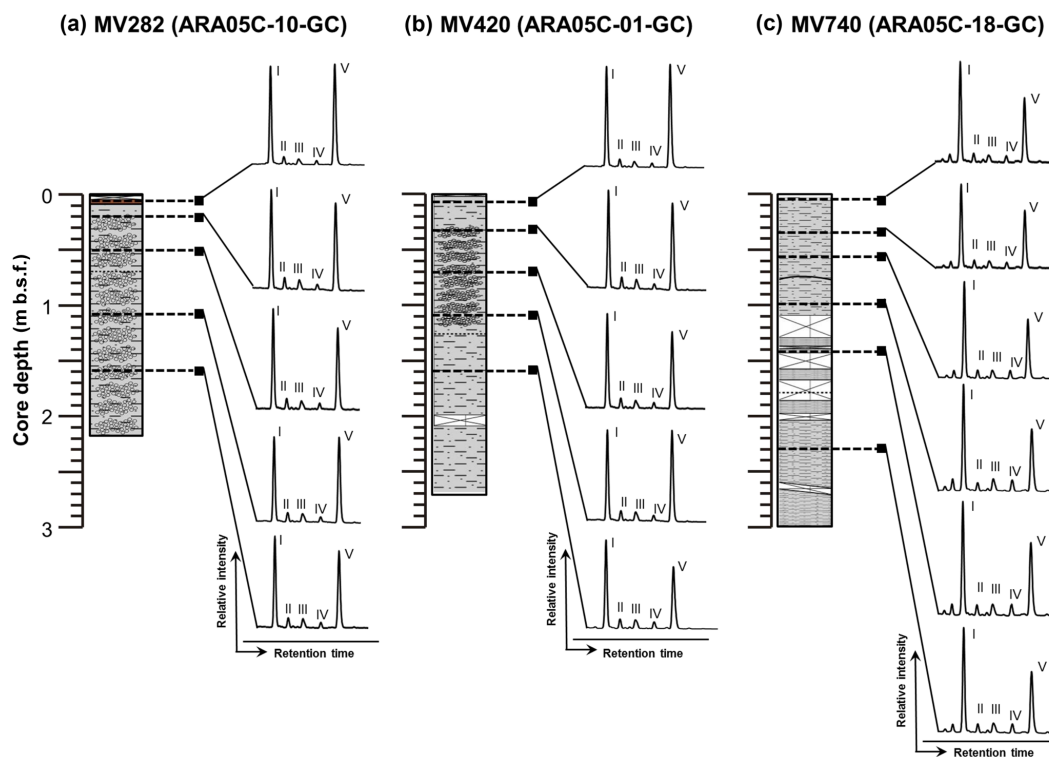
Figure 4. HPLC-MS base peak chromatograms of polar fractions obtained from sediment cores **(a)** ARA05C-10-GC (MV282), **(b)** ARA05C-01-GC (MV420), and **(c)** ARA05C-18-GC (MV740). Note that the Roman numerals (I, II, III, IV, and V) refer to GDGT-0, GDGT-1, GDGT-2, GDGT-3, and crenarchaeol, respectively. The Arabic numbers in GDGT-0, GDGT-1, GDGT-2, and GDGT-3 indicate the number of cyclopentane rings within the biphytane chains.

sn-2-hydroxyarchaeol has only been found in certain orders of methanogens such as Methanosarcinales, Methanococcales, Methanopyrales, Thermoplasmatales, Sulfolobales, and Methanomicrobiales (e.g., Kushwaha and Kates, 1978; Koga et al., 1993, 1998; Koga and Morii, 2005), and *sn*-3-hydroxyarchaeol has been detected in Methanosarcinales (*Methanosaeta concilii*) and Methanococcales (*Methanococcus voltae*; Ferrante et al., 1988; Sprott et al., 1993).

Microbial communities dominated by ANME-2 at the cold seeps of the northwestern Black Sea contained higher amounts of *sn*-2-hydroxyarchaeol relative to archaeol, whereas the reverse was observed in microbial mats dominated by ANME-1 (Blumenberg et al., 2004). Indeed, the ratio of isotopically depleted *sn*-2-hydroxyarchaeol relative to archaeol can be used to distinguish ANME-1 (0–0.8) from ANME-2 (1.1–5.5), with ANME-3 (2.4) falling within the range of ANME-2 (Niemann et al., 2006; Niemann and Elvert, 2008). In our dataset, the concentration of *sn*-2-hydroxyarchaeol was slightly higher than that of archaeol in MV282 but lower in MV420 and MV740 (Fig. 3; see also Table 1). Accordingly, the *sn*-2-hydroxyarchaeol / archaeol ratio was between 1.3 and 1.8 in MV282 but below 0.7 for most of the samples from MV420 and MV740, except for at depths of 0.7 m (1.4) in MV420 and 0.4–0.6 m (0.9–1.1)

in MV740 (Fig. 3; see also Table 1). This observation suggests that ANME-2 (or ANME-3) was involved in AOM in MV282, whereas ANME-1 was probably involved in AOM in MV420 and MV740, except for at the depths mentioned above.

However, the $\delta^{13}C$ values of archaeol were, on average, $-62.6\,‰$ in MV282, $-49.4\,‰$ in MV420, and $-54.3\,‰$ in MV740, except for at 0.7 m in MV420 ($-79.8\,‰$). Hence, the $\delta^{13}C$ values of archaeol in most of the MV sediments appeared to be enriched in ^{13}C in comparison to that of the ascending methane in the MVs (about $-64\,‰$; Paull et al., 2015), indicating admixture from processes other than AOM. Hence, it appears that the ratio of *sn*-2-hydroxyarchaeol to archaeol was generally high in all investigated MVs, hinting at a negligible involvement of ANME-1 in AOM, even in MV420 and MV740. Previous studies showed that GDGTs were mostly absent in ANME-2-dominated settings but not in ANME-1-dominated settings, which typically contain substantial amounts of GDGT-1 and GDGT-2 (e.g., Blumenberg et al., 2004; Stadnitskaia et al., 2008a, b; Chevalier et al., 2011; Kaneko et al., 2013). The GDGT distributions found here (Fig. 4) indeed show a clear dominance of GDGT-0 and crenarchaeol over GDGT-1 and GDGT-2. Hence, our lipid data indicate that ANME-2 and/or ANME-3 are involved in

AOM in the Beaufort Sea MVs, rather than ANME-1. We did not detect crocetane, which is diagnostic for ANME-2 (Elvert et al., 1999), but we also found no PMIs which are structurally similar to crocetane and produced by ANME-1, ANME-2, and ANME-3 (Niemann and Elvert, 2008), so we could not carry out a further chemotaxonomic distinction of the dominant ANME groups.

4.3.2 Nucleic acid-based phylogeny

To further identify key AOM communities, we investigated the archaeal community by pyrosequencing of 16S rRNA genes. In line with geochemical and biomarker signals for AOM in the surface sediments of the investigated MVs, we found archaeal sequences of the Methanomicrobia, which contains the order Methanosarcinales (i.e., the clade to which the ANME archaea also belong) at higher abundances in the upper depths of the MV sediment cores than the lower depths (see Supplement Table S2 and Fig. S2). To further clarify the phylogenetic position within the class Methanomicrobia (comprising both methanogens and methanotrophs), phylogenies of the three most dominant (more than 1 % of all archaeal sequences) Methanomicrobia OTUs (c116, c1698, and c1784) were inferred from 16S rRNA gene sequences (Table S2). The OTU c116 represented 2.5 %–14.1 % and 0.2 %–6.7 % of the archaeal sequences at core depths of 0.0–0.2 m in MV282 and 0.1–1.1 m in MV420, respectively, whereas this OTU was less than 0.2 % at MV740 (Table S2). The OTU c1698 accounted for more than 1 % of the archaeal sequences at the surface of MV282 but was absent at other MVs. The OTU c1784 accounted for 1.2 %–6.8 % and 3.7 %–14.9 % of the archaeal sequences at core depths of 0.0–0.2 m in MV282 and 0.4–0.6 m in MV740, respectively. In contrast, this OTU was rarely detected at all depths of MV420, except for at the depth of 0.7 m. The OTUs c116 and c1698 belonged to the ANME-3 archaeal lineage, and the OTU c1784 formed a cluster with sequences of ANME-2c, a distinct lineage of Methanosarcinales (Fig. 5). Hence, the occurrence of these sequences, together with our lipid data, provides evidence that the AOM communities belong to the ANME-2 and ANME-3 clades; ANME-1 does not seem to play a role at the investigated Beaufort Sea MVs. In line with our geochemical and lipid analyses, the abundance of ANME sequences was also low, underscoring that the contribution of the AOM communities to the archaeal biomass at the MVs investigated here was rather minor. Instead, we found that most archaeal sequences belong to the MCG_c clade (up to 99.2 % of all sequences) within the phylum Bathyarchaeota. Although members of this clade were previously shown to perhaps be involved in methane oxidation in marine and estuary settings (Inagaki et al., 2006; Jiang et al., 2011; Li et al., 2012), little is known about their physiology and biogeochemical roles in nature.

4.4 Mechanism controlling microbial communities in Beaufort Sea mud volcanoes

16S rRNA signatures from the Beaufort Sea MVs revealed the presence of AOM related to ANME-2 and ANME-3, albeit in relatively low proportions (Fig. 5). The ANME-2 can be divided into three subgroups: ANME-2a, ANME-2b, and ANME-2c (e.g., Orphan et al., 2001; Knittel et al., 2005). In the Beaufort Sea MVs, the ANME-2c subgroup was detected (Fig. 5). A previous study at Hydrate Ridge (Cascadia margin off the coast of Oregon, USA) showed that ANME-2c was dominant at symbiotic clam *Calyptogena* sites, accounting for > 75 % of the total ANME-2, whereas ANME-2a was the most abundant at a site covered by the sulfide-oxidizing bacterium *Beggiatoa*, accounting for up to 80 % (Knittel et al., 2005). Fluid flow rates and the methane fluxes from the seafloor were substantially weaker at *Calyptogena* sites than at *Beggiatoa* sites (e.g., Tryon et al., 1999; Sahling et al., 2002). The distinct distribution of ANME-2 subgroups might reflect their sulfide tolerance and oxygen sensitivity (Roalkvam et al., 2011). It appears that ANME-2c has a preferential niche, interacting with chemosynthetic habitats in relatively low methane fluxes in the Beaufort Sea MVs.

The thermal gradients in our study area (see Paull et al., 2015) were substantially higher in the MVs (517.7 mK m^{-1} in MV282, 557.9 mK m^{-1} in MV420, and 104.3 mK m^{-1} in MV740) than in the reference site (28.9 mK m^{-1}). In general, high geothermal gradients were observed where methane emission activities were high, as reported at the Dvurechenskii MV (Feseker et al., 2009) and the Haakon Mosby MV (Kaul et al., 2006). Accordingly, among the MV sites, the methane flux appeared to be the highest at the MV420 site. Indeed, we found a lower abundance of ANME-2c in MV420 than in MV282 and MV740 (Fig. 5; see also Table S2). The MV740 site had the lowest thermal gradient of the MV sites and thus probably the lowest methane flux, which is consistent with the presence of the gas hydrate flake at 230 cm in the MV740 sediment core (see Fig. 1d). At this MV site, ANME-2c occurred at a deeper core depth (0.3–0.7 m) than at the MV282 site (0.0–0.3 m; see also Table S2). This might be linked to the lower methane flux at the MV740 site than at the MV282 site, resulting in penetration of sulfate to deeper sediment depths. Notably, at active MV sites, the sulfate penetration depth can be limited to the upper 2 cm sediment layers (cf. Niemann et al., 2006).

Besides ANME-2c, 16S rRNA gene analyses also revealed the presence of ANME-3 (see Table S2). Notably, ANME-3 occurred in MV420, whereas thermal gradients were high (indicating high methane flux), and ANME-2c was almost absent. However, ANME-3 was absent in MV740 where ANME-2c was present. Similar to ANME-2a, ANME-3 was previously found at a site with high fluid flow and a high methane flux, associated with *Beggiatoa* mats at the Haakon Mosby mud volcano located in the Barents Sea at the water depth of 1250 m (Niemann et al., 2006; Lösekann et al.,
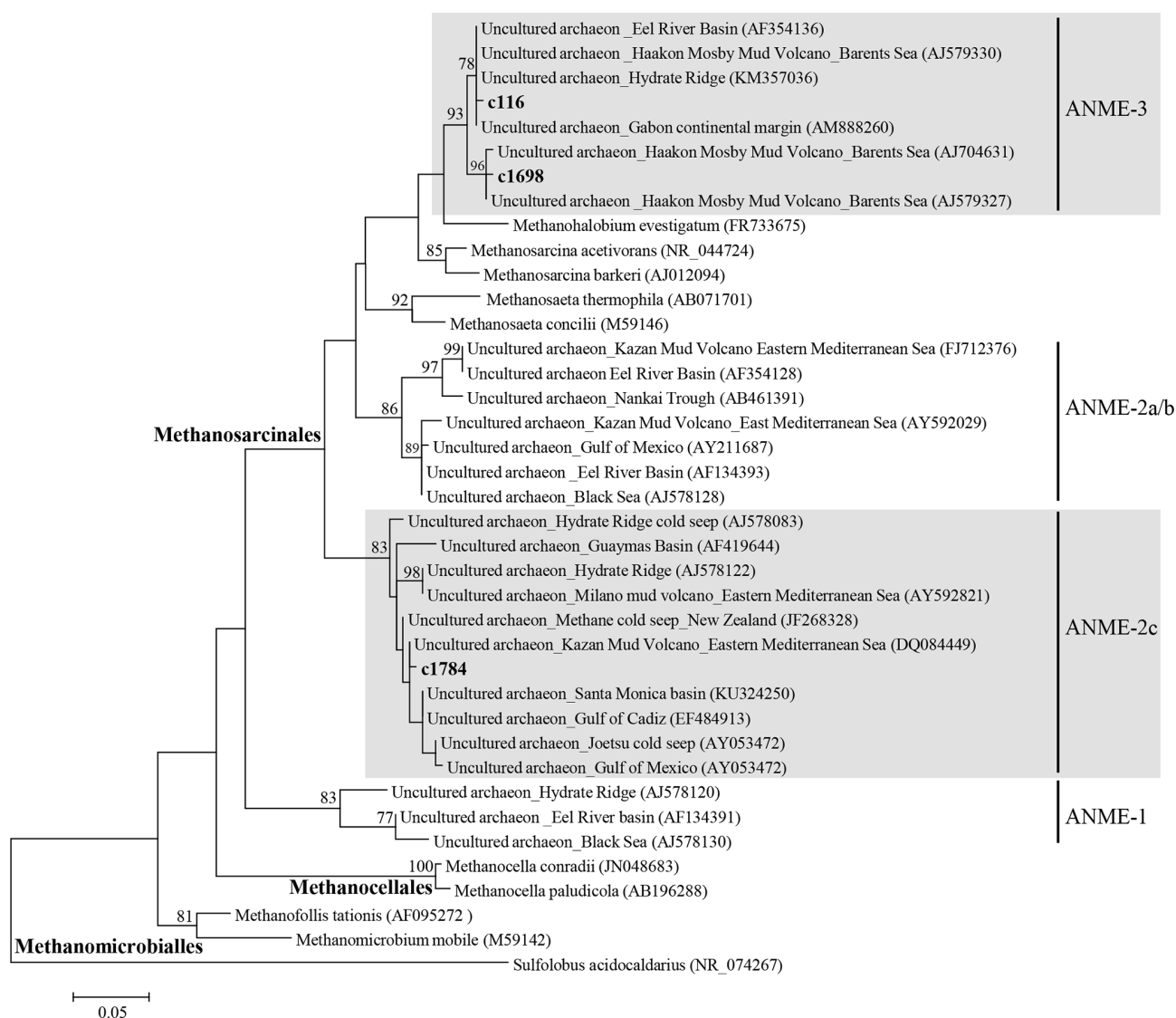
Figure 5. Phylogenetic tree based on 16S rRNA, showing the relationships of methanomicrobial sequences recovered in this study with selected reference sequences of the phylum Euryarchaeota. The phylogenetic tree was inferred by the maximum likelihood method. Bootstrap values of > 70 are shown on corresponding branches. The scale bar indicates evolutionary distance of 0.05 substitutions per site.

2007). Accordingly, it seems that ANME-3 thrives better in a setting with higher methane fluxes than ANME-2c.

5 Summary and conclusions

Integrated biogeochemical and nucleic acid analyses were performed for three sediment cores retrieved from active MVs in the Beaufort Sea. The sharp decrease in pore water sulfate concentrations and steep thermal gradients and previous observations of gas flare above the edifices indicate that sulfate-depleted warm fluids and methane ascend from the Beaufort Sea MVs. We found isotopically depleted lipid biomarkers and nucleic acid signatures of microbial communities, most likely ANME-2c and ANME-3, mediating AOM

in the surface sediments at these MVs. The prevalence of ANME-3 over ANME-2c at sites characterized by high thermal gradients (and thus probably high methane fluxes) provides a further indication of a methane-flux driven niche segregation of these ANME-clades. However, the overall contribution of AOM-related biomass to the organic carbon pool was rather low, and the presence of dominant amounts of lipid biomarkers with comparably high ^{13}C values, as well as the dominance of non-ANME sequences, underscores the importance of processes other than AOM in the sediments of the MVs investigated here. Given that our gravity coring system failed to recover the uppermost surface sediments, preventing us from detecting the most active AOM occurrences in the Beaufort Sea MVs, further studies should investigate

the undisturbed uppermost surface sediments to investigate the diversity and distribution of AOM-related archaeal communities in detail and to clarify their preferred habitats in the Beaufort Sea MV systems, for instance, using ROV push cores.

References

Abbas, B., Coolen, M. J. L., Hopmans, E. C., Baas, M., van Weering, T. C. E., Ivanov, M. K., Poludetkina, E., and Sinninghe Damsté, J. S.: Biomarker and 16S rDNA evidence for anaerobic oxidation of methane and related carbonate precipitation in deep-sea mud volcanoes of the Sorokin Trough, Black Sea, Mar. Geol., 217, 67–96, 2005.

Akhmanov, G. G.: Lithology of mud breccia clasts from the Mediterranean Ridge, Mar. Geol., 132, 151–164, 1996.

Akhmanov, G. G. and Woodside, J. M.: Mud Volcanic samples in the content of the Mediterranean Ridge Mud Diapiric Belt, in: Proceed- ings of the ODP, Scientific Results, edited by: Robert-son, A. H. F., Emeis, K.-C., Richter, C., and Camerlenghi, A., College Station, Texas, Vol. 160, 597–605, 1998.

Beal, E. J., House, C. H., and Orphan, V. J.: Manganese- and iron-dependent marine methane oxidation, Science, 325, 184–187, 2009.

Blasco, S., Bennett, R., Brent, T., Burton, M., Campbell, P., Carr, E., Covill, R., Dallimore, S., Davies, E., Hughes-Clarke, J., Issler, D., MacKillop, K., Mazzotti, S., Patton, E., Shearer, J., and White, M.: 2010 state of knowledge: Beaufort Sea seabed geo-hazards associated with offshore hydrocarbon development, Geological Survey of Canada Open File 6989, 340 pp., 2013.

Blumenberg, M., Seifert, R., Reitner, J., Pape, T., and Michaelis, W.: Membrane lipid patterns typify distinct anaerobic methanotrophic consortia, P. Natl. Acad. Sci. USA, 101, 11111–11116, 2004.

Boetius, A. and Wenzhöfer, F.: Seafloor oxygen consumption fuelled by methane from cold seeps, Nat. Geosci., 6, 725–734, 2013.

Boetius, A., Ravenschlag, K., Schubert, C. J., Rickert, D., Widdel, F., Gieseke, A., Amann, R., Jørgensen, B. B., Witte, U., and Pfannkuche, O.: A marine microbial consortium apparently mediating anaerobic oxidation of methane, Nature, 407, 623–626, 2000.

Bradley, A. S., Hayes, J. M., and Summons, R. E.: Extraordinary ^{13}C enrichment of diether lipids at the Lost City Hydrothermal Field indicates a carbon-limited ecosystem, Geochim. Cosmochim. Ac., 73, 102–118, 2009.

Campbell, P., Carr, E., Beaton, F., and Blasco, S. M.: 2009 Beaufort Sea seabed mapping program – operations report, Draft report prepared by Canadian seabed research Ltd. for the geological survey of Canada, 2009.

Chevalier, N., Bouloubassi, I., Birgel, D., Cremiere, A., Taphanel, M. H., and Pierre, C.: Authigenic carbonates at cold seeps in the Marmara Sea (Turkey): a lipid biomarker and stable carbon and oxygen isotope investigation, Mar. Geol., 288, 112–121, 2011.

Chevalier, N., Bouloubassi, I., Stadnitskaia, A., Taphanel, M. H., and Sinninghe Damsté, J. S.: Lipid biomarkers for anaerobic oxidation of methane and sulphate reduction in cold seep sediments of Nyegga pockmarks (Norwegian margin): Discrepancies in contents and carbon isotope signatures, Geo-Mar. Lett., 34, 269–280, 2014.

De Rosa, M. and Gambacorta, A.: The Lipids of archaebacteria, Prog. Lipid Res., 27, 153–175, 1988.

Edgar, R. C., Haas, B. J., Clemente, J. C., Quince, C., and Knight, R.: UCHIME improves sensitivity and speed of chimera detection, Bioinformatics, 27, 2194–2200, 2011.

Elvert, M., Suess, E., and Whiticar, M. J.: Anaerobic methane oxidation associated with marine gas hydrates: superlight C-isotopes from saturated and unsaturated C_{20} and C_{25} irregular isoprenoids, Naturwissenschaften, 86, 295–300, 1999.

Elvert, M., Hopmans, E. C., Treude, T., Boetius, A., and Suess, E.: Spatial variations of methanotrophic consortia at cold methane seeps: implications from a high-resolution molecular and isotopic approach, Geobiology, 3, 195–209, 2005.

Etminan, M., Myhre, G., Highwood, E. J., and Shine, K. P.: Radiative forcing of carbon dioxide, methane, and nitrous oxide: A significant revision of the methane radiative forcing, Geophys. Res. Lett., 43, 12614–12623, 2016.

Felden, J., Wenzhöfer, F., Feseker, T., and Boetius, A.: Transport and consumption of oxygen and methane in different habitats of the Håkon Mosby Mud Volcano (HMMV), Limnol. Oceanogr., 55, 2366–2380, 2010.

Felden, J., Ruff, S. E., Ertefai, T., Inagaki, F., and Hinrichs, K.: Anaerobic methanotrophic community of a 5346-m-deep vesicomyid clam colony in the Japan Trench, Geobiology, 12, 183–199, 2014.

Felsenstein, J.: Evolutionary Trees from DNA Sequences?: A Maximum Likelihood Approach, J. Mol. Evol., 17, 368–376, 1981.

Ferrante, G., Ekiel, I., Patel, G. B., and Sprott, G. D.: A novel core lipid isolated from the aceticlastic methanogen, *Methanothrix concilii* GP6, Biochim. Biophys. Acta, 963, 173–182, 1988.

Feseker, T., Pape, T., Wallmann, K., Klapp, S. A., Schmidt-Schierhorn, F., and Bohrmann, G.: The thermal structure of the Dvurechenskii mud volcano and its implications for gas hydrate stability and eruption dynamics, Mar. Pet. Geol., 26, 1812–1823, 2009.

Haese, R. R., Meile, C., Van Cappellen, P., and De Lange, G. J.: Carbon geochemistry of cold seeps: Methane fluxes and transformation in sediments from Kazan mud volcano, eastern Mediterranean Sea, Earth Planet. Sc. Lett., 212, 361–375, 2003.

Haroon, M. F., Hu, S., Shi, Y., Imelfort, M., Keller, J., Hugenholtz, P., Yuan, Z., and Tyson, G. W.: Anaerobic oxidation of methane coupled to nitrate reduction in a novel archaeal lineage, Nature, 500, 567–570, 2013.

Himmler, T., Birgel, D., Bayon, G., Pape, T., Ge, L., Bohrmann, G., and Peckmann, J.: Formation of seep carbonates along the Makran convergent margin, northern Arabian Sea and a molecular and isotopic approach to constrain the carbon isotopic composition of parent methane, Chem. Geol., 415, 102–117, 2015.

Hinrichs, K. U. and Boetius, A.: The anaerobic oxidation of methane: new insights in microbial ecology and biogeochemistry, edited by: Wefer, G., Billett, D., Hebbeln, D., Jørgensen, B. B., Schlüter, M., and Van Weering, T., Springer-Verlag, Berlin, Germany, 2002.

Huguet, C., Hopmans, E. C., Febo-Ayala, W., Thompson, D. H., Sinninghe Damsté, J. S., and Schouten, S.: An improved method to determine the absolute abundance of glycerol dibiphytanyl glycerol tetraether lipids, Org. Geochem., 37, 1036–1041, 2006.

Hwang, K., Oh, J., Kim, T. K., Kim, B. K., Yu, D. S., Hou, B. K., Caetano-Anollés, G., Hong, S. G., and Kim, K. M.: CLUSTOM: a novel method for clustering 16S rRNA next generation sequences by overlap minimization, PLoS One, 8, e62623, https://doi.org/10.1371/journal.pone.0062623, 2013.

Inagaki, F., Nunoura, T., Nakagawa, S., Teske, A., Lever, M., Lauer, A., Suzuki, M., Takai, K., Delwiche, M., Colwell, F. S., Nealson, K. H., Horikoshi, K., D'Hondt, S., and Jorgensen, B. B.: Biogeographical distribution and diversity of microbes in methane hydrate-bearing deep marine sediments on the Pacific Ocean Margin, P. Natl. Acad. Sci. USA, 103, 2815–2820, 2006.

Ivanov, M. K., Limonov, A. F., and Woodside, J. M.: Geological and geophysical investigations in the Mediterranean and Black Seas, Initial results of the "Training-through-Research" Cruise of R/V *Gelendzhik* in the Eastern Mediterranean and the Black Sea (June/July 1991), UNESCO Reports in Marine Sciences, 56, 208 pp., 1992.

Ivanov, M. K., Limonov, A. F., and Woodside, J. M.: Extensive deep fluid flux through the sea floor on the Crimean continental margin

(Black Sea), in: Gas Hydrate, Relevance to World Margin Stability and Climatic Change, edited by: Henriet, J.-P. and Mienert, J., Geological Society, London, Special Publications, Vol. 137, 195–213, 1998.

James, R. H., Bousquet, P., Bussmann, I., Haeckel, M., Kipfer, R., Leifer, I., Niemann, H., Ostrovsky, I., Piskozub, J., Rehder, G., Treude, T., Vielstädte, L., and Greinert, J.: Effects of climate change on methane emissions from seafloor sediments in the Arctic Ocean: A review, Limnol. Oceanogr., 61, 283–299, 2016.

Jiang, L., Zheng, Y., Chen, J., Xiao, X., and Wang, F.: Stratification of archaeal communities in shallow sediments of the Pearl River Estuary, Southern China, Antonie van Leeuwenhoek, Int. J. Gen. Mol. Microbiol., 99, 739–751, 2011.

Kaneko, M., Kitajima, F., and Naraoka, H.: Stable hydrogen isotope measurement of archaeal ether-bound hydrocarbons, Org. Geochem., 42, 166–172, 2011.

Kaneko, M., Naraoka, H., Takano, Y., and Ohkouchi, N.: Distribution and isotopic signatures of archaeal lipid biomarkers associated with gas hydrate occurrences on the northern Cascadia Margin, Chem. Geol., 343, 76–84, 2013.

Kaul, N., Foucher, J. P., and Heesemann, M.: Estimating mud expulsion rates from temperature measurements on Håkon Mosby Mud Volcano, SW Barents Sea, Mar. Geol., 229, 1–14, 2006.

Kim, J., Lee, D., Yoon, S., Jeong, K., Choi, B., and Shin, K.: Chemosphere Contribution of petroleum-derived organic carbon to sedimentary organic carbon pool in the eastern Yellow Sea (the northwestern Pacific), Chemosphere, 168, 1389–1399, 2017.

Kim, O. S., Cho, Y. J., Lee, K., Yoon, S. H., Kim, M., Na, H., Park, S. C., Jeon, Y. S., Lee, J. H., Yi, H., Won, S., and Chun, J.: Introducing EzTaxon-e: A prokaryotic 16s rRNA gene sequence database with phylotypes that represent uncultured species, Int. J. Syst. Evol. Microbiol., 62, 716–721, 2012.

Knittel, K. and Boetius, A.: Anaerobic oxidation of methane: Progress with an unknown process, Annu. Rev. Microbiol., 63, 311–334, 2009.

Knittel, K., Lösekann, T., Boetius, A., Kort, R., Amann, R., and Lo, T.: Diversity and Distribution of Methanotrophic Archaea at Cold Seeps Diversity and Distribution of Methanotrophic Archaea at Cold Seeps, Appl. Environ. Microbiol., 71, 467–479, 2005.

Koga, Y. and Morii, H.: Recent Advances in Structural Research on Ether Lipids from Archaea Including Comparative and Physiological Aspects, Biosci. Biotechnol. Biochem., 69, 2019–2034, 2005.

Koga, Y., Nishihara, M., Morii, H., and Akagawa-Matsushita, M.: Ether polar lipids of methanogenic bacteria: Structures, comparative aspects, and biosyntheses, Microbiol. Rev., 57, 164–182, 1993.

Koga, Y., Morii, H., Akagawa-Matsushita, M., and Ohga, M.: Correlation of Polar Lipid Composition with 16S rRNA Phylogeny in Methanogens, Further Analysis of Lipid Component Parts, Biosci. Biotechnol. Biochem., 62, 230–236, 1998.

Kopf, A. J.: Significance of mud volcanism, Rev. Geophys., 40, 2–46, 2002.

Kushwaha, S. C. and Kates, M.: 2, 3-Di-O-phytanyl-sn-glycerol and prenols from extremely halophilic bacteria, Phytochemistry, 17, 2029–2030, 1978.

Lee, D. H., Kim, J. H., Bahk, J. J., Cho, H. Y., Hyun, J. H., and Shin, K. H.: Geochemical signature related to lipid biomarkers of

ANMEs in gas hydrate-bearing sediments in the Ulleung Basin, East Sea (Korea), Mar. Pet. Geol., 47, 125–135, 2013.

Levitus, S., Antonov, J. I., Boyer, T. P., and Stephens, C.: Warming of the world ocean, Science, 287, 2225–2229, 2000.

Li, Q., Wang, F., Chen, Z., Yin, X., and Xiao, X.: Stratified active archaeal communities in the sediments of Jiulong River estuary, China, Front. Microbiol., 3, 1–14, 2012.

Liu, X., Lipp, J. S., and Hinrichs, K.-U.: Distribution of intact and core GDGTs in marine sediments, Org. Geochem., 42, 368–375, 2011.

Lösekann, T., Knittel, K., Nadalig, T., Fuchs, B., Niemann, H., Boetius, A., and Amann, R.: Diversity and Abundance of Aerobic and Anaerobic Methane Oxidizers at the Haakon Mosby Mud Volcano, Barents Sea, Appl. Environ. Microbiol., 73, 3348–3362, 2007.

Marín-Moreno, H., Giustiniani, M., Tinivella, U., and Piñero, E.: The challenges of quantifying the carbon stored in Arctic marine gas hydrate, Mar. Pet. Geol., 71, 76–82, 2016.

Milkov, A. V., Sassen, R., Apanasovich, T. V., and Dadashev, F. G.: Global gas flux from mud volcanoes: A significant source of fossil methane in the atmosphere and the ocean, Geophys. Res. Lett., 30, 17–20, 2003.

Milucka, J., Ferdelman, T. G., Polerecky, L., Franzke, D., Wegner, G., Schmid, M., Lieberwirth, I., Wagner, M., Widdel, F., and Kuyper, M. M. M.: Zero-valent sulphur is a key intermediate in marine methane oxidation, Nature, 491, 541–546, 2012.

Nauhaus, K., Albrecht, M., Elvert, M., Boetius, A., and Widdel, F.: In vitro cell growth of marine archaeal-bacterial consortia during anaerobic oxidation of methane with sulfate, Environ. Microbiol., 9, 187–196, 2007.

Niemann, H. and Elvert, M.: Diagnostic lipid biomarker and stable carbon isotope signatures of microbial communities mediating the anaerobic oxidation of methane with sulphate, Org. Geochem., 39, 1668–1677, 2008.

Niemann, H., Elvert, M., Hovland, M., Orcutt, B., Judd, A., Suck, I., Gutt, J., Joye, S., Damm, E., Finster, K., and Boetius, A.: Methane emission and consumption at a North Sea gas seep (Tommeliten area), Biogeosciences, 2, 335–351, https://doi.org/10.5194/bg-2-335-2005, 2005.

Niemann, H., Lösekann, T., de Beer, D., Elvert, M., Nadalig, T., Knittel, K., Amann, R., Sauter, E. J., Schlüter, M., Klages, M., Foucher, J. P., and Boetius, A.: Novel microbial communities of the Haakon Mosby mud volcano and their role as a methane sink, Nature, 443, 854–858, 2006.

Oh, J., Kim, B. K., Cho, W. S., Hong, S. G., and Kim, K. M.: PyroTrimmer: A software with GUI for pre-processing 454 amplicon sequences, J. Microbiol., 50, 766–769, 2012.

Orphan, V. J., Hinrichs, K., Iii, W. U., Paull, C. K., Taylor, L. T., Sylva, S. P., Hayes, J. M., and Delong, E. F.: Comparative Analysis of Methane-Oxidizing Archaea and Sulfate-Reducing Bacteria in Anoxic Marine Sediments, Appl. Environ. Microbiol., 67, 1922–1934, 2001.

Pancost, R. D., Sinninghe Damsté, J. S., Lint, S. D., van der Maarel, M. J. E. C., Gottschal, J. C., and Shipboard Scientific Party: Biomarker evidence for widespread anaerobic methane oxidation in Mediterranean sediments by a consortium of methanogenic archaea and bacteria, Appl. Environ. Microbiol., 66, 1126–1132, 2000.

Pancost, R. D., Bouloubassi, I., Aloisi, G., and Sinninghe Damsté, J. S.: Three series of non-isoprenoidal dialkyl glycerol diethers in cold-seep carbonate crusts, Org. Geochem., 32, 695–707, 2001a.

Pancost, R. D., Hopmans, E. C., Sinninghe Damsté, J. S., and Shipboard Scientific Party: Archaeal lipids in mediterranean cold seeps: Molecular proxies for anaerobic methane oxidation, Geochim. Cosmochim. Ac., 65, 1611–1627, 2001b.

Pancost, R. D., McClymont, E. L., Bingham, E. M., Roberts, Z., Charman, D. J., Hornibrook, E. R. C., Blundell, A., Chambers, F. M., Lim, K. L. H., and Evershed, R. P.: Archaeol as a methanogen biomarker in ombrotrophic bogs, Org. Geochem., 42, 1279–1287, 2011.

Paull, C. K., Dallimore, S., Hughes, J., Blasco, S., Lundsten, E., Ussler III, W., Graves, D., Sherman, A., Conway, K., Melling, H., Vagle, S., and Collett, T.: Tracking the decomposition of submarine permafrost and gas hydrate under the shelf and slope of the Beaufort Sea, Proceedings of the 7th International Conference on Gas Hydrates, 1, 1689–1699, 2011.

Paull, C. K., Dallimore, S. R., Caress, D. W., Gwiazda, R., Melling, H., Riedel, M., Jin, Y. K., Hong, J. K., Kim, Y.-G., Graves, D., Sherman, A., Lundsten, E., Anderson, K., Lundsten, L., Villinger, H., Kopf, A., Johnson, S. B., Clarke, J. H., Blas, S., Conway, K., Neelands, P., Thomas, H., and Cote, M.: Active mud volcanoes on the continental slope of the Canadian Beaufort Sea, Geochem. Geophy. Geosy., 16, 1541–1576, 2015.

Polyakov, I. V., Timokhov, L. A., Alexeev, V. A., Bacon, S., Dmitrenko, I. A., Fortier, L., Frolov, I. E., Gascard, J.-C., Hansen, E., Ivanov, V. V., Laxon, S., Mauritzen, C., Perovich, D., Shimada, K., Simmons, H. L., Sokolov, V. T., Steele, M., and Toole, J.: Arctic Ocean Warming Contributes to Reduced Polar Ice Cap, J. Phys. Oceanogr., 40, 2743–2756, 2010.

Reeburgh, W. S.: Oceanic Methane Biogeochemistry, Chem. Rev., 107, 486–513, 2007.

Roalkvam, I., Jørgensen, S. L., Chen, Y., Stokke, R., Dahle, H., Hocking, W. P., Lanzén, A., Haflidason, H., and Steen, I. H.: New insight into stratification of anaerobic methanotrophs in cold seep sediments, FEMS Microbiol. Ecol., 78, 233–243, 2011.

Rossel, P. E., Elvert, M., Ramette, A., Boetius, A., and Hinrichs, K. U.: Factors controlling the distribution of anaerobic methanotrophic communities in marine environments: Evidence from intact polar membrane lipids, Geochim. Cosmochim. Ac., 75, 164–184, 2011.

Sahling, H., Rickert, D., Lee, R. W., Linke, P., and Suess, E.: Macrofaunal community structure and sulfide flux at gas hydrate deposits from the Cascadia convergent margin, NE Pacific, Mar. Ecol. Prog. Ser., 231, 121–138, 2002.

Saint-Ange, F., Kuus, P., Blasco, S., Piper, D. J. W., Hughes, J., and Mackillop, K.: Multiple failure styles related to shallow gas and fluid venting, upper slope Canadian Beaufort Sea, northern Canada, Mar. Geol., 355, 136–149, 2014.

Schouten, S., Huguet, C., Hopmans, E. C., Kienhuis, M. V. M., and Sinninghe Damsté, J. S.: Analytical methodology for TEX$_{86}$ paleothermometry by high-performance liquid chromatography/atmospheric pressure chemical ionization-mass spectrometry, Anal. Chem., 79, 2940–2944, 2007.

Schouten, S., Hopmans, E. C., and Sinninghe Damsté, J. S.: The organic geochemistry of glycerol dialkyl glycerol tetraether lipids?: a review, Org. Geochem., 54, 19–61, 2013.

Shnukov, E. F., Starostenko, V. I., Rusakov, O. M., Kobolev, V. P., and Maslakov, N. A.: Gas volcanism in the Black Sea. Abstract. International Workshop on Methane in Sediments and Water Column of the Black Sea: Formation, Transport, Pathways and the Role Within the Carbon Cycle, Sevastopol, Ukraine, 50–51, 2005.

Sprott, G. D., Dicaire, C. J., Choquet, C. G., Patel, G. B., Ekiel, I., and Dennis, G.: Hydroxydiether Lipid Structures in Hydroxydiether Lipid Structures in Methanosarcina Methanococcus voltaet, Appl. Environ. Microbiol., 59, 912–914, 1993.

Stadnitskaia, A., Muyzer, G., Abbas, B., Coolen, M. J. L., Hopmans, E. C., Baas, M., van Weering, T. C. E., Ivanov, M. K., Poludetkina, E., and Sinninghe Damsté, J. S.: Biomarker and 16S rDNA evidence for anaerobic oxidation of methane and related carbonate precipitation in deep-sea mud volcanoes of the Sorokin Trough, Black Sea, Mar. Geol., 217, 67–96, 2005.

Stadnitskaia, A., Ivanov, M. K., and Damsté, J. S. S.: Application of lipid biomarkers to detect sources of organic matter in mud volcano deposits and post-eruptional methanotrophic processes in the Gulf of Cadiz, NE Atlantic, Mar. Geol., 255, 1–14, 2008a.

Stadnitskaia, A., Nadezhkin, D., Abbas, B., Blinova, V., Ivanov, M. K., and Damste, J. S. S.: Carbonate formation by anaerobic oxidation of methane: Evidence from lipid biomarker and fossil 16S rDNA, Geochim. Cosmochim. Ac., 72, 1824–1836, 2008b.

Tamura, K., Stecher, G., Peterson, D., Filipski, A., and Kumar, S.: MEGA6: Molecular evolutionary genetics analysis version 6.0, Mol. Biol. Evol., 30, 2725–2729, 2013.

Tryon, M. D., Brown, K. M., Torres, M. E., Tréhu, A. M., McManus, J., and Collier, R. W.: Measurements of transience and downward fluid flow near episodic methane gas vents, Hydrate Ridge, Cascadia, Geology, 27, 1075–1078, 1999.

Weijers, J. W. H., Lim, K. L. H., Aquilina, A., Sinninghe Damsté, J. S., and Pancost, R. D.: Biogeochemical controls on glycerol dialkyl glycerol tetraether lipid distributions in sediments characterized by diffusive methane flux, Geochem. Geophy. Geosy., 12, Q10010, https://doi.org/10.1029/2011GC003724, 2011.

Werne, J., Baas, B., and Damsté, J. S. S.: Molecular isotopic tracing of carbon flow and trophic relationships in a methane supported microbial community, Limnol. Oceanogr., 47, 1694–1701, 2002.

Werne, J. P., Haese, R. R., Zitter, T., Aloisi, G., Bouloubassi, I., Heijs, S., Fiala-Médioni, A., Pancost, R. D., Sinninghe Damsté, J. S., de Lange, G., Forney, L. J., Gottschal, J. C., Foucher, J. P., Mascle, J., and Woodside, J.: Life at cold seeps: A synthesis of biogeochemical and ecological data from Kazan mud volcano, eastern Mediterranean Sea, Chem. Geol., 205, 367–390, 2004.

Westbrook, G. K., Thatcher, K. E., Rohling, E. J., Piotrowski, A. M., Pälike, H., Osborne, A. H., Nisbet, E. G., Minshull, T. A., Lanoisellé, M., James, R. H., Hühnerbach, V., Green, D., Fisher, R. E., Crocker, A. J., Chabert, A., Bolton, C., Beszczynska-Möller, A., Berndt, C., and Aquilina, A.: Escape of methane gas from the seabed along the West Spitsbergen continental margin, Geophys. Res. Lett., 36, 1–5, 2009.

Whiticar, M. J.: Carbon and hydrogen isotope systematics of bacterial formation and oxidation of methane, Chem. Geol., 161, 291–314, 1999.

Wuebbles, D. J. and Hayhoe, K.: Atmospheric methane and global change, Earth-Sci. Rev., 57, 177–210, 2002.

Zhang, C. L., Pancost, R. D., Sassen, R., Qian, Y., and Macko, S. A.: Archaeal lipid biomarkers and isotopic evidence of anaerobic methane oxidation associated with gas hydrates in the Gulf of Mexico, Org. Geochem., 34, 827–836, 2003.

Zhang, Y. G., Zhang, C. L., Liu, X.-L., Li, L., Hinrichs, K.-U., and Noakes, J. E.: Methane Index: A tetraether archaeal lipid biomarker indicator for detecting the instability of marine gas hydrates, Earth Planet. Sc. Lett., 307, 525–534, 2011.